SAND84 — 0824
Unlimited Release
Printed July 1984

Distribution
Category UC — 70

Strategic Petroleum Reserve Acoustical Emissions Experiment at Bayou Choctaw

H. Douglas Garbin
Ground Motion and Seismic Division 7111
Sandia National Laboratories
Albuquerque, NM 87185

Abstract

In March 1982, Sandia National Laboratories (SNL) conducted a pressurization experiment in a salt dome at the Bayou Choctaw facility near Baton Rouge, LA. Three, three-axis geophones were installed to monitor the acoustic emission activity produced by the pressurization cycle. Difficulties with cultural and environmental noise produced many alarms (800). No acoustic emission events were identified. The downhole package produced resonances that distorted the signals. As a result, if any events had been identified, this difficulty would have precluded quantitative determination of locations and magnitudes.

Contents

Figures

Tables

Strategic Petroleum Reserve Acoustical Emissions Experiment at Bayou Choctaw

Introduction

During 1981 – 1982, Sandia National Laboratories (SNL) conducted a seismic experiment at the Department of Energy (DOE) Bayou Choctaw petroleum storage facility near Baton Rouge, LA (Figure 1). The purpose was to monitor the seismic activity during a pressurization-depressurixation cycle of a salt cavern to characterize the local activity and any significant deformations during the pressurization cycle.

Figure 1. Bayou Choctaw SPR Site Location Map

Los Alamos National Laboratory (LANL) performed a similar experiment in November 1978, at Bryan Mound Salt Dome located near Freeport, *TX*.' There were several major differences between these two experiments:

- The LANL experiment used one triaxial geophone system, whereas the SNL experiment used three triaxial geophones.
- LANL recorded the data only on an analog tape, while SNL recorded on analog tape and used a data acquisition system with an event detector and recorded the events digitally.
- The geometry of the Bayou Choctaw Cavern is a simple cylinder, and Bryan Mound Cavern is rather irregular, resembling two cells with a pinch-off between them (Figures 2 and 3).

The SNL experiment attempted to expand the results of the LANL experiment and develop an on-line seismic monitoring system. This required the study of

- Seismicity
- Activity location
- Activity magnitude

Experimental Plan

A seismic net of geophones was placed in nearby holes surrounding Well 2, the pressurization cavern. Figure 4 details the Bayou Choctaw site and Cavern 2. Triaxial geophones occupied Well 4 to the east, Well 1 to the southwest, and Borehole 1 to the north. In addition, Well 2 had 'a vertical geophone operating during the quiescent times in which no pressurization was being performed. Table 1 lists the depths and ranges of the geophones with respect to the Cavern 2 wellhead.

Strategic Petroleum Reserve Acoustical Emissions Experiment at Bayou Choctaw

Introduction

During 1981 – 1982, Sandia National Laboratories (SNL) conducted a seismic experiment at the Department of Energy (DOE) Bayou Choctaw petroleum storage facility near Baton Rouge, LA (Figure 1). The purpose was to monitor the seismic activity during a pressurization-depressurixation cycle of a salt cavern to characterize the local activity and any significant deformations during the pressurization cycle.

Figure 1. Bayou Choctaw SPR Site Location Map

Los Alamos National Laboratory (LANL) performed a similar experiment in November 1978, at Bryan Mound Salt Dome located near Freeport, *TX*.' There were several major differences between these two experiments:

- The LANL experiment used one triaxial geophone system, whereas the SNL experiment used three triaxial geophones.
- LANL recorded the data only on an analog tape, while SNL recorded on analog tape and used a data acquisition system with an event detector and recorded the events digitally.
- The geometry of the Bayou Choctaw Cavern is a simple cylinder, and Bryan Mound Cavern is rather irregular, resembling two cells with a pinch-off between them (Figures 2 and 3).

The SNL experiment attempted to expand the results of the LANL experiment and develop an on-line seismic monitoring system. This required the study of

- Seismicity
- Activity location
- Activity magnitude

Experimental Plan

A seismic net of geophones was placed in nearby holes surrounding Well 2, the pressurization cavern. Figure 4 details the Bayou Choctaw site and Cavern 2. Triaxial geophones occupied Well 4 to the east, Well 1 to the southwest, and Borehole 1 to the north. In addition, Well 2 had 'a vertical geophone operating during the quiescent times in which no pressurization was being performed. Table 1 lists the depths and ranges of the geophones with respect to the Cavern 2 wellhead.

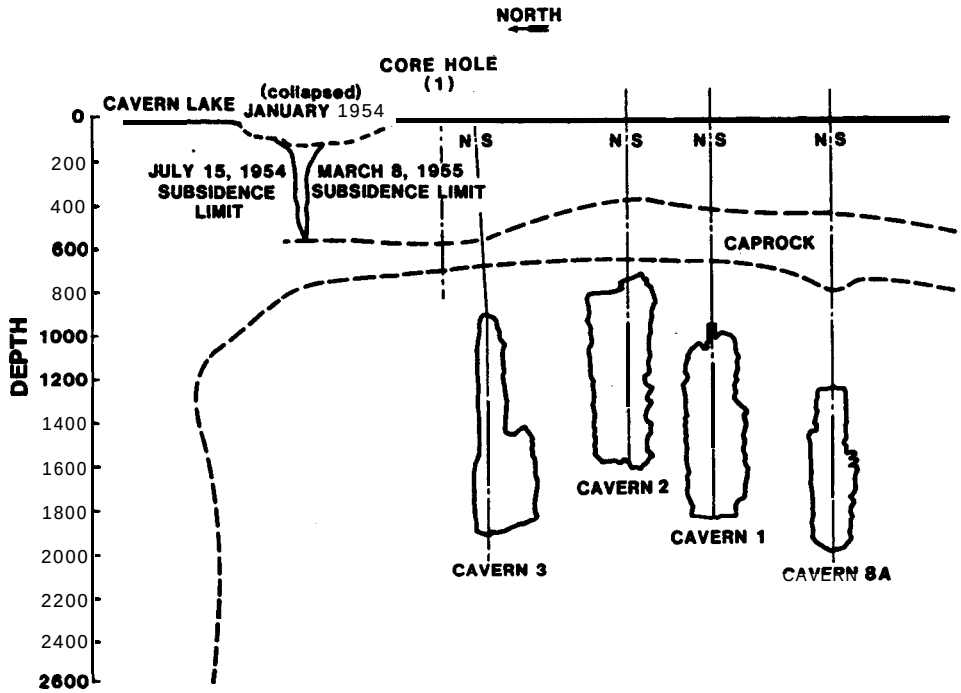

Figure 5. North-South Profile of Bayou Choctaw SPR Sits

Note that the Well 4 geophone package was in the caprock. The hole terminated at this point because a plug was located -570 ft beneath the surface. The other geophones were positioned in salt-in the case of Well 1, just above the cavern. The idea was to keep the geophones away from reflecting surfaces so that, if required, a single-station analysis could be applied using the back azimuth to locate small events, i.e., to minimize the effects of any scattering. The Well 1 geophone was positioned 920 ft deep in an attempt to get some depth resolution in the location determinations.

The pressurization cycle took place between February 20 and March 26. Ideally, the entire cycle consisted of five parts. First, before pressurization, a baseline of seismicity was determined (7-10 days). The actual pressurization of Cavern 2 with brine required about 1 day. The cavern would then remain pressurized for a week until the depressurixation phase (2 days, as shown in Figure 6) and the final quiet post-test monitoring (4-7 days).

This schedule was essentially followed. However, the pressurization phase was not completed in a single step as a continuous brine flow could not be obtained. A pressure of -100 psi was attained in the first step, and a wellhead pressure of -215 psi was reached -4 days later.

Instrumentation

Figure 7 is a schematic of the triaxial geophone package used at Bayou Choctaw. The system includes the six geophones (orthogonal pairs are connected in parallel to enhance the signal), downhole amplifiers, and a locking system. The geophones were Geo Space HS-1 Model K with a natural frequency of 4.5 Hz. The asymptotic response of the geophones for frequencies of -40 Hz is 0.51 (V/in./s). The downhole amplifiers had gains of 2000. Additional uphole amplifiers in the instrument trailer could further amplify the signal The locking system consisted of an arm that extended out and pushed against the side of the hole. The package was lowered to the desired depth, where a command activated the arm coupling the entire package to the side of the hole.

Three filters were applied to the signal. First, a low-pass analog filter with a cutoff frequency of 5 KHz was applied. The signal was then passed through an additional 2 KHz low-pass digital filter. The sample rate for each recording channel was -4167 (50 000/12) samples per second. An additional 30 Hz high-pass filter was available if excessive cultural noise was in evidence. This latter filter usually was used only during daytime operations, when cultural noise was often excessive.

Table 2. Bayou Choctaw SPR Site: Caprock Ultrasonic Velocities*

Boring Number	Depth† (ft)	S-Wave Velocity (fps) $\sigma_a=0$	a =500 $\sigma_a=1000$	$\sigma_a=2000$	a,=3000	p-Wave Velocity (fps) $\sigma_a=0$	a =500 $\sigma_a=1000$	a,=2000	a,=3000
DOE CH1	602.5	10 007	10 152	10 202	10 430 —	16 975	17 184	17 326	17 470 —
	645.75	7 624	9 308	9 645	9883 10 007	17 032	18 616	19 525	19 525 19 525
	. 648.05	7980	8 704	8 818	8 911 —	17 053	17 870	18 874	19 198 —
	648.4	7 305	7 501	7569	7 569 —	16 849	17 464	17 464	17 647 —
Mean Value		8 229	8 916	9 059	9 198 10 007	16 977	17 784	18 297	18 460 19 525
Std Dev		1 213	1 115	1 144	1255 —	92	622	1077	1052 —
DOE CH2	558.0					3 425	5 538	8 209	
	566.0					2 854	5 187	6 582	
	566.15					3 438	5 384	11 441	
	582.1					15 407	16 763	16 946	
	606.11					6 050	9 797	16 444	
	634.7					16 704	17 009	17 009	
	635.13					17 143	17 537	17 671	
	635.63					16 215	16 392	16 569	
Mean Value						10 155	11701	13 859	
Std Dev						6 725	5 779	4 452	

		$\sigma_h=0$	$\sigma_h=500$	$\sigma_h=1000$	$\sigma_h=2500$
DOE CH2	634.33	16 585	16 736	16 966	17 045
	641.58	16 851	17 147	17 301	17 376
	642.25	—	16 589	—	—
Mean Value		16 718	16 824	17 134	17 211
std Dev		188	289	237	234

*Modified from Dames & Moore, 1978.

'Depth below rotating Kelly bushing, which was 15 ft above ground surface.

a,= Axial stress in psi.

σ_h = Hydrostatic stress in psi.

Table 3. Bayou Choctaw SPR Site: Salt Ultrasonic Velocities

Boring Number	Depth† (ft)	S-Wave Velocity (fps)				p-Wave Velocity (fps)			
		$\sigma_a=0$	$\sigma_a=500$	$\sigma_a=1000$	$\sigma_a=1500$	$\sigma_a=0$	$\sigma_a=500$	$\sigma_a=1000$	$\sigma_a=1500$
BC1	714.1	—	—	—	—	14 591	14 653	14 715	14 970
	714.6	7507	7 773	7 927	8 006	14 735	14 827	15 496	16 120
	714.95	—	—	—	—	15 165	15 301	15 370	15 439
	715.5	8 117	8 212	8386	8 488	14 020	14 765	15 086	15 772
	715.85	8 032	8 944	9 305	9 751	14 856	14 856	14 919	14 984
	716.4	7 799	8 288	8 439	8 570	16 210	16 372	16 453	16 536
	716.7	9 210	9 630	9 909	10 056	14 608	14 671	14 800	15 546
	722.2	8790	9 679	9 761	9 928	15 492	15 775	16 219	16 373
	722.9	8005	8 143	8 285	8 367	14 495	14 621	14 685	14 685
Mean Value		8 209	8 667	8 859	9 024	14 908	15 093	15 305	15 603
Std Dev		589	759	787	854	641	610	650	653

†Depth below rotating Kelly bushing, which was 15 ft above ground surface.

σ_a = Axial stress in psi.

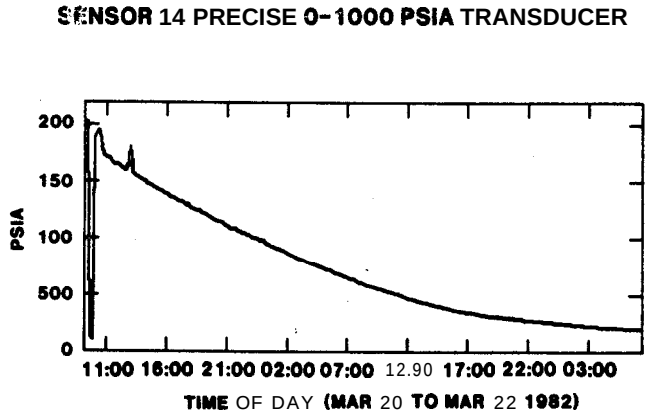

Figure 6. Depressurization History Recorded at Wellhead 2

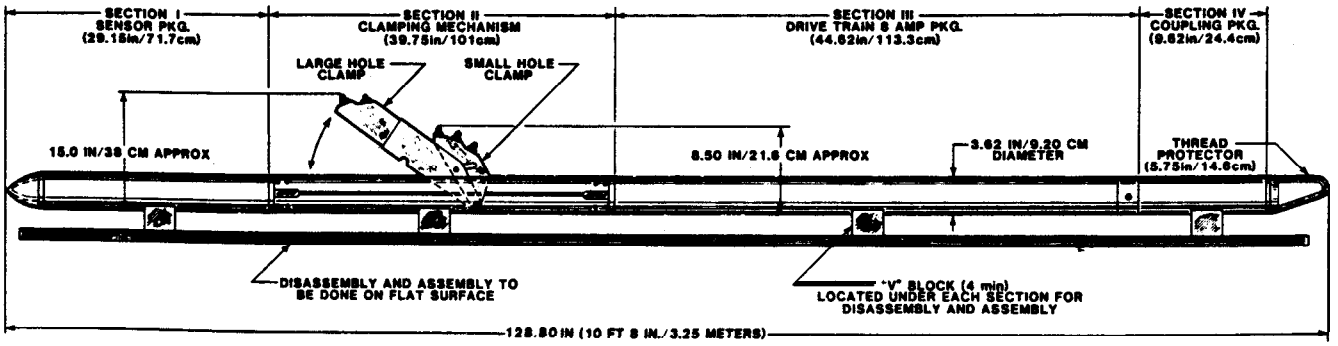

Figure 7. Downhole Geophone Package

The instrument trailer allowed us to record in two modes.[2] Two analog tape drives recorded continuously during the experiment. Each tape provided **16 hr** of data, with -1 hr of overlap between each tape; i.e., when one tape was almost finished, the second tape drive would begin recording.

In addition to the analog recordings, event-detected signals were digitized by an HP-1000 mini-computer in an 8-s time window around the event. If the signal passed two detection tests, the event was written on tape. The first test used a microprocessor with an algorithm based on a long-term, short-term average ratio of the sum of absolute amplitudes of a channel. Three different channels could be monitored simultaneously for this phase of event detection. This was a first, quick pass at detection; if a channel passed this first test, a more extensive, leisurely test was initiated by the computer. The second test consisted of a long-term, short-term average ratio of the squared amplitudes; if the event passed this test, all channels were recorded on digital tape. The computer has the capacity to have up to 10 events on disc.

Pretest Analysis

I hoped to study three important features in this experiment: **(1)** frequency of occurrence, (2) location, and (3) size of the induced acoustic emissions created by the pressure cycle. To aid in this analysis, many calibration detonations were made. Because the locations and times of these events were known, this allowed for the calculation of velocities and the determination of the orientation of the horizontal geophones. When the geophones were lowered and clamped into the various holes, it was not possible to know how the radial and tangential components were aligned. The orientation and average seismic velocities are, of course, required for single-station, event-location analysis. We were able to determine the media velocities; however, the orientation is in doubt.

Figure 4 shows the Strategic Petroleum Reserve (SPR) well and hole locations. **Figure** 5 is a side view of the salt dome along a north-south line. There were two detonation experiments, however, only the last is described as an example. This included the shooting of **1.5-** and 3.5-g detonators at depths of 600 and 700 ft above Cavern 2. Seven detonations were made; Table 4 lists the **size** and depth of each event. The data were high-pass filtered to eliminate the offset voltage (Figure 8).

Table 4. Shot Size and Location in Well 2

Shot No.	Depth (ft)	Size (g)
1	**700**	**3.5**
2	**600**	**3.5**
3	**700**	**3.5**
4	**600**	**3.5**
5	**700**	DUD
6	**700**	**3.5**
7	**600**	1.5

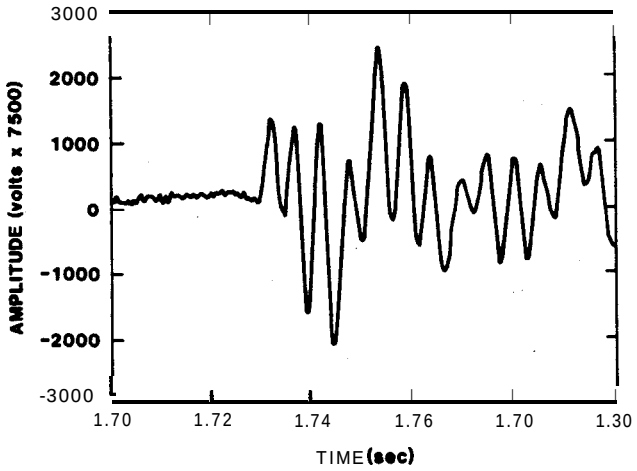

Figure 8. **Tangential Signal Recorded on Well 4 Channel**

The data from the Well 1 hole had the least system noise in all three of its components. The results of the average velocity calculations are given in Table 5. The velocities for Well 1 hole and **Borehole 1** for the **700-ft** detonation are almost identical, which indicates a relatively homogeneous salt medium at depths between 700 and 920 ft. The average velocity for Well 4 hole for thii **700-ft** detonation is higher because of the higher velocity in the overlying **caprock** (salt-caprock interface is at -640 ft deep). If a layered medium is assumed, the interface depth can be calculated from the detonation time data, it is estimated to be at 637 ft (Appendix A). These velocities are reasonable and compare favorably with previous ultrasonic studies.

Table 5. Average Velocity Results for Various Geophones and Events

Shot Depth (ft)	Geophone	V_1 (ft/s)
700	Well 4	16 235
700	Well 1	14 485
700	Borehole 1	14 515
600	Well 4 hole	16 897
600	Well 1 hole	15 272

Although the velocities obtained are reasonable, determining the orientation of the three components of each geophone package is not as promising. To illustrate the problem, results from the Well 1 geophone follow. All three components in this system are relatively noise free and have a high signal-to-noise ratio (SNR). This is not true with the other geophone systems, so the Well 1 results should be the best case.

Consider the geophone coordinate system in Figure 9. (X,Y,Z) is the geophone coordinate system. (X^1,Y^1,Z^1) is the earth coordinate system (i.e., X^1 points east), and r gives the direction of the incident p-wave. The azimuthal (ϕ) and polar (19) angles are determined from the vector sum of the three-component geophone signals. Since both the source and receiver locations are known, both θ^1 and ϕ^1 can be calculated from the usual spherical coordinate transformations, and thus, the geophone coordinate system can be rotated ϕ-ϕ^1 to align with the earth's coordinate system. Since the angle of inclination of the well holes does not vary much with respect to the vertical, θ should be the same for both coordinate systems; i.e., the z-axis is the same for both systems.

There were three 3.5-g detonators shot at a depth of 700 ft in Well 1. The events were very reproducible, so each component was high-pass filtered (– 3dB at 400 Hz) and added to the corresponding component (stacked) to reduce noise by $1/\sqrt{3}$. The resulting wave forms are shown in Figures 10 – 12 and the corresponding hodographs of the initial phase in Figures 13 and 14.

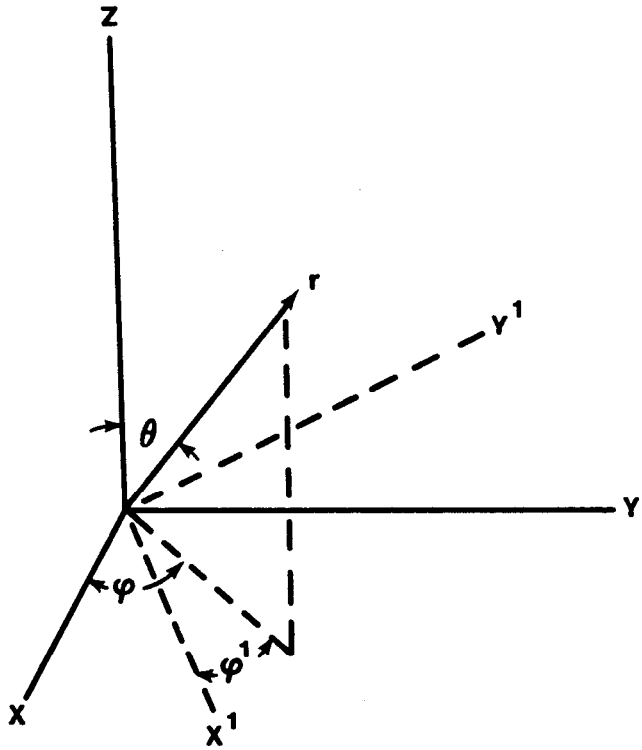

Figure 9. Rotations Defining Angles in the Earth and Geophone Coordinate Systems

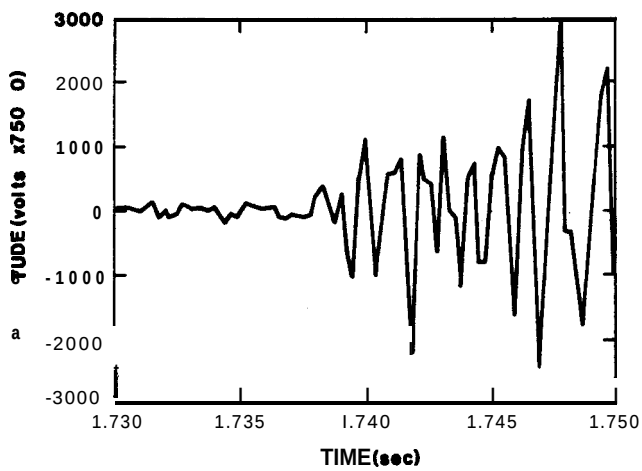

Figure 10. Stacked Vertical Signal From Geophone in Well 2

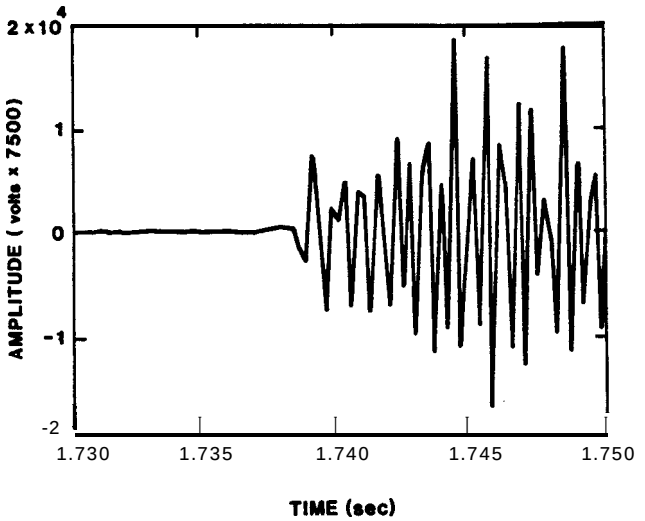

Figure 11. Stacked Tangential Signal From Geophone in Well 2

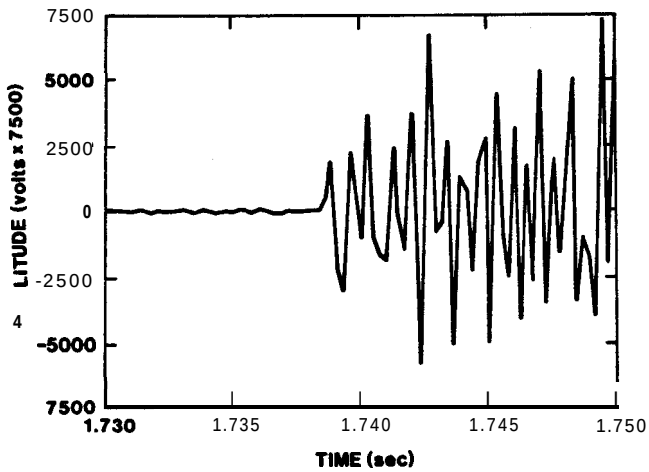

Figure 12. Stacked Radial Signal From Geophone in Well 2

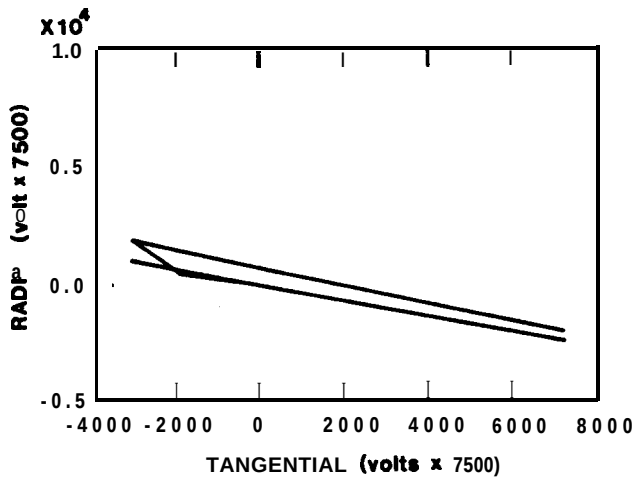

Figure 13. Hodograph for Horizontal Components

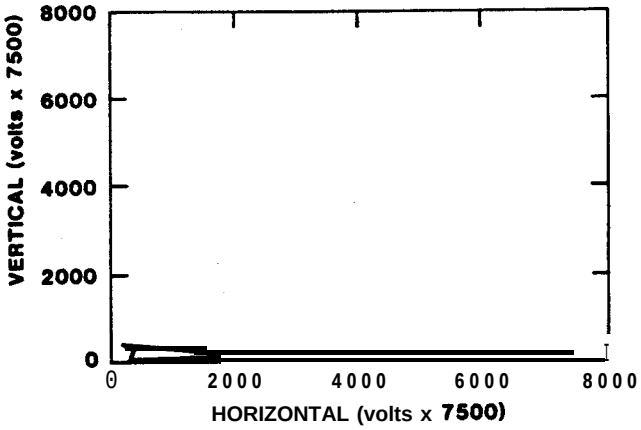

Figure 14. Hodograph for Vertical Components

A regression analysis over the first two peaks of the first arrival was done to calculate a statistical average for the angles ϕ and θ. The average was weighted to the sum of the square amplitudes of the total signal. The result of this regression analysis is

$$\phi = -0.3151 \pm 0.0113 \text{ rad, and}$$

$$\theta = 1.525 \pm 0.004 \text{ rad.} \quad (1)$$

There is no way to verity whether ϕ is correct; however, θ is the same for both coordinate systems. Thus, as a check using the coordinate system defined in Table 1, we can calculate what θ should be from the geometry of the experiment. Assuming a straight-line ray path,

$$\theta = \cos^{-1}(z/R) = \cos^{-1}\left(\frac{220}{490}\right) \approx 1.105 \text{ rad.} \quad (2)$$

From **Eq** (1) and **(2),** we see there is a **0.42-rad** discrepancy from the **direct** path value. Note that the rms deviations are $\ll$ 0.42 rad, indicating that the signal is emitted from a consistent source. Also, the **0.42-rad** difference translates to a **200-ft** error at a range of 500 ft.

There are several possible causes for these deviations. However, low **SNRs** and unknown layering, which plague the other geophone packages, are not a problem here. Diffraction off caverns, causing interference, is certainly a possibility, but if this were the case, one would expect the hodographs to be more erratic. Also, the Well 1 geophone is at SO – 100 ft from the cavern ceiling, which translates into at least a 0.01-s delay with respect to the arrival time. This is well outside the first cycle of the first arrival. Diffraction off Cavern 2 occurs, but its effect is unknown. Mechanical coupling of the **downhole** package along

with electronic system problems can also produce confusing signals.

In an attempt to pinpoint the trouble, the entire seismic system, from the wellheads to the computer, was checked for possible problems. Identical electronic signals were compared after being transmitted through the three orthogonal channels from the wellheads to the computer. Amplitude and phase-transfer functions were found to be in good agreement. Figures 15-17 are representative spectral plots from Borehole 1 of white noise signals low-pass filtered at 1000 Hz. Figures 18 and 19 are the spectral ratios of these transmitted signals. Note that the amplitude ratios and phase differences are close to 1 and 0, respectively. This implies that the anomalous effects are due to the downhole package.

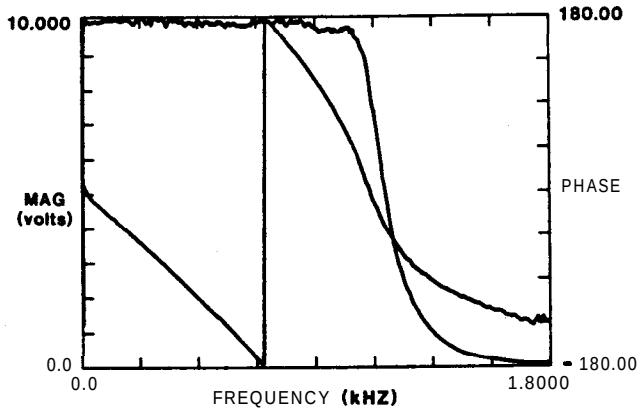

Figure 17. Spectrum Recorded at Trailer of White Noise Signal Generated in the Radial Channel at Wellhead 1

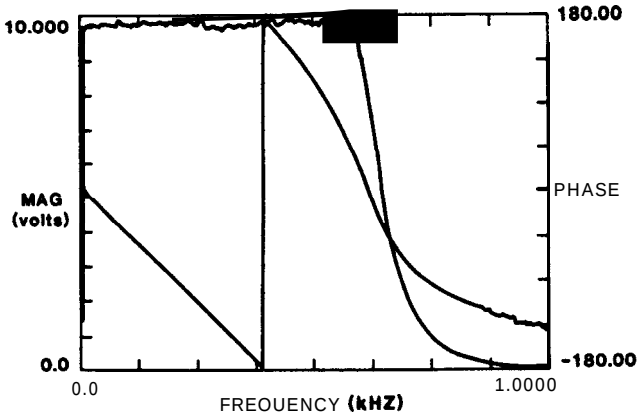

Figure 15. Spectrum Recorded at Trailer of White Noise Signal Generated in the Vertical **Channel** at **Wellhead 1**

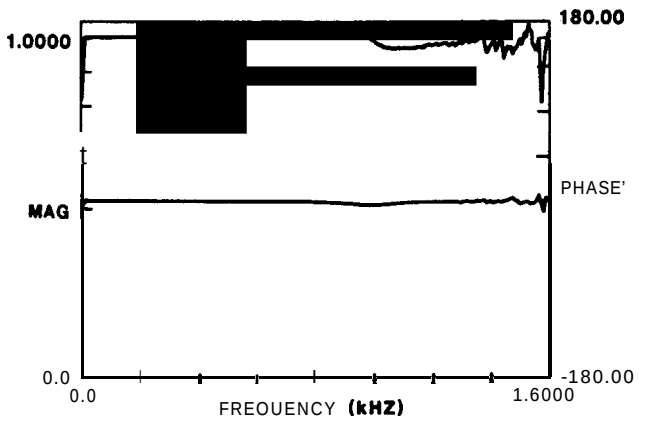

Figure 18. Ratio of Vertical to Radial White Noise Spectra

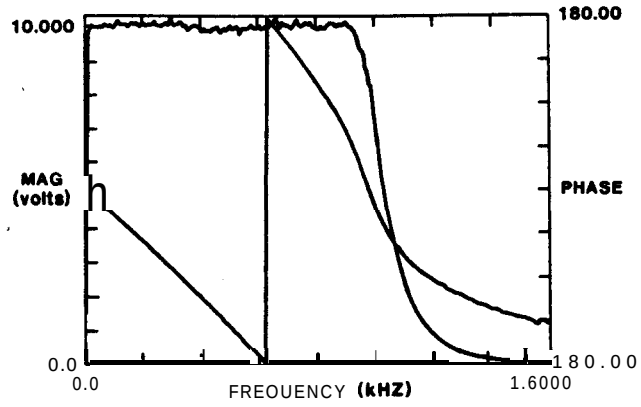

Figure 16. Spectrum Recorded at Trailer of White Noise Signal Generated in the Tangential Channel at Wellhead 1

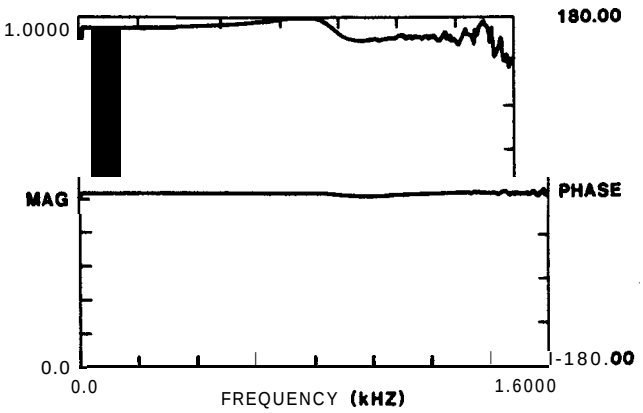

Figure 19. Ratio of Tangential to Radial White Noise Spectra

Velocity variations in the salt could refract the initial arrival, so it appears to be incident from a steeper angle. However, the velocities calculated from Borehole 1 and Well 1 first arrivals are very close. This indicates a homogeneous salt velocity with depth. If a velocity-depth relationship of the form $C = C_o + G \cdot Z$ is assumed, then a velocity of 22 000 ft/s is required at 920 ft deep to obtain the polar incident angle determined from the hodographs. This is an unreasonably high velocity for salt.

In addition, the azimuthal angles are not consistent. Detonators were ignited in Wells 1 and 2. The hodograph records of the Well 4 data should have a 32° difference in the horizontal angles. The records were noisy, so they were filtered at various bandpasses where the signal was above the noise. No 32° angular difference could be found; in fact, the angular discrepancy from the 32° was 69°.

Mechanical coupling of the geophone package most likely caused the difficulties. As another illustration of the geophones' anomalous behavior, the horizontal components of an event are shown in Figures 20 and 21. Note that the tangential response has a much lower frequency content in the first arrival than the radial component. The horizontal components are configured such that the tangential component is normal to the clamping arm, and the radial component is parallel to it. It is possible that different frequency modes associated with the geophone package configuration are excited in each horizontal component. The wavelengths of interest are about the length of the geophone package. These induced modes mask the true ground motion. If a lower frequency source were used, this problem would not be important.

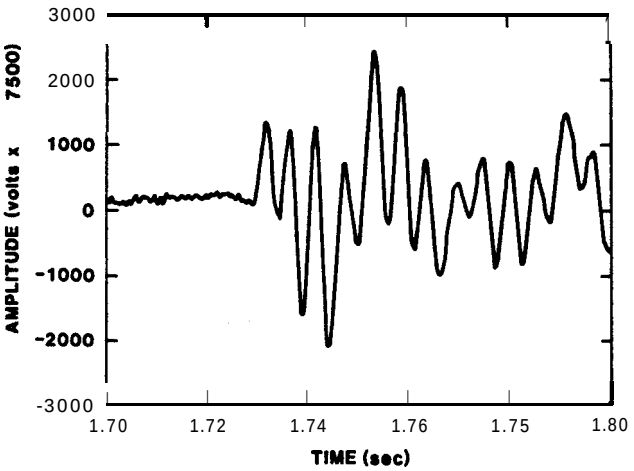

Figure 20. Tangential Signal Recorded on Well 4 Channel

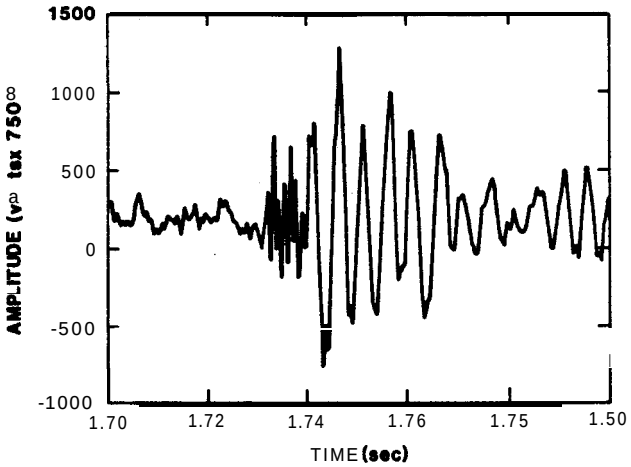

Figure 21. Radial Signal Recorded on Well 4 Channel

Appendix B shows an analysis of a vibrating beam, which supports the conclusion that the clamping arm of the instrument package has the resonant frequencies contaminating the signals. Many of the possible resonance frequencies of the clamping arm are prominent in the records.

Results

Because of the difficulties described, the analysis program is greatly curtailed. The frequency anomalies preclude any analyses using back azimuths for event location or the Brune spectral models[3] for source size. The only study that can be reasonably attempted is seismicity, but even this study has some difficulties related to the false-alarm rate.

There were 800 alarms during the pressurization cycle, but no acoustic emission events could be identified. Of the 600 alarms, 450 were triggered by the geophone located in the pressurization Cavern 2 (this geophone was not used during pressurization or depressurixation). This channel was discovered to be sensitive to wind noise and was triggered often during gusty periods by a tarpaulin striking a connector. Table 6 is a log of events illustrating the problem. From the table, it can be seen that triggers 11 s apart were not unusual. It appears that the winds coupled with the wellhead geophone connectors resulted in an electrical response. Because of the difficulties with this channel, any response that triggered the channel was not considered.

Table 6. Event Log During Windy Period:* Well 2 Geophone Trigger (9)

Event	Elapsed Time Into Test	Time	Trigger
338	84:37:54	20:27:28	9
339	84:38:05	20:27:39	9
340	84:38:17	20:27:51	9
341	84:38:30	20:28:04	9
342	84:38:44	20:28:18	9
343	84:39:19	20:28:53	9
344	84:39:34	20:29:08	9
345	84:40:21	20:29:55	9
346	84:40:32	20:30:06	9
347	84:42:44	20:32:18	9
348	84:43:00	20:32:34	9
349	84:43:18	20:32:52	9
350	84:44:11	20:33:45	9
351	84:44:37	20:34:11	9
352	84:44:57	20:34:31	9
353	84:45:10	20:34:44	9
354	84:46:19	20:35:53	9
355	84:47:11	20:36:45	9
356	84:51:50	20:41:24	9
357	84:52:58	20:42:32	9
358	84:53:18	20:42:52	9
359	84:54:48	20:44:22	9
366	84:55:00	20:44:34	9
361	84:56:23	20:45:57	9
362	84:57:31	20:47:05	9
363	84:58:18	20:47:52	9

'March 25, 1982

Most of the remaining events (triggers) were due to cultural and environmental noise, such as trucks operating in the area, lightning, pumps, and explosives. From the site map (Figure 4), it can be seen that there were ample opportunities for introduction of cultural noise into the seismic experiment. A road that runs just east of Cavern 2 is used extensively by heavy trucks hauling machinery. This traffic was detected on Borehole 1, Well 1, and Well 2 geophones. Large pumps located about 50 ft north of Borehole 1 were operated at odd hours, affecting detection performance. Also, various operations were conducted near a brine pond located just east of Well 4. Finally, drilling just across the north-south canal to the west of Well 2 was detected on all geophones.

I plotted and visually scanned all the recorded signals except those from the geophone in Cavern 2, as previously noted. The criteria used to identify events consisted of noting the signal frequency characteristics and times of arrival. Cultural noise was identified by the long-duration, low-frequency wave trains (15 to 20 Hz). Many of these signals were present on a surface geophone located near the Cavern 4 wellhead. I did not expect to see small acoustical emission events on a surface geophone because of the velocity contrasts of the overlying geology. Lightning produced obvious irregular nonseismic signals. Explosive events were common in the area and, when known, were noted as such on the event log. Otherwise, explosive events were eliminated from consideration by time-of-arrival arguments.

The false alarms are more than a nuisance. When enough of them occur, they can cause blind spots in the monitoring. This can result in two ways: a large false-alarm rate and numerous false alarms occurring overnight.

To explain the first case, it should be noted that the disc can record a maximum of 10 events. If new events trigger the initial event detector at a high rate; when the disc is full, the new events are not recorded. Thus, such events are "lost" before the second event detection test is applied or before a valid event can be recorded on tape. This should not happen, but with the large number of false alarms, the system simply can be saturated.

The second difficulty arises because only two tape drives are available. Two tapes are mounted each night, and if there are a large number of false alarms (56), these tapes could be completely filled, resulting in no more events being recorded on tape until new tapes were mounted in the morning.

With these trigger sources identified, I was unable to find acoustical emission events during the experiment. Because of the event-detecting difficulties described, some events may not have been recorded. I have no idea whether any events were overwritten on the disc. However, this seems highly improbable because scans of the tape logs showed that the times of possible saturation were not long in duration. In addition, at no time were two tapes-expended completely during a single night. Thus, I believe no events were missed. There is one other possible seismicity error—the analyst error. I scanned more than 800 events, and

my interpretation of acoustic emission events vs cultural noise could be faulty. Scanning so many records is long, boring, and tedious work, and I may have missed some events.

Although we detected no events, the LANL experiment found a total of 1'7 micro-earthquakes during depressurization. This possibly could be due to the in situ stress field. Our cavity was much less complicated, with fewer irregularities than the LANL cavity. High stress concentrations about irregularities could trigger more events, in fact, many of the LANL events occurred in the area between the upper and lower cells (Figure 2). In a finite element model analysis, LANL postulates a possible micro-earthquake mechanism as a result of the formation of localized regions of increased creep rate caused by the depressurixation. In regions of already high stress fields, this effect could trigger the events. However, if the stress field is somewhat diffused, as in our case, it is possible for no events to be triggered.

Although no acoustical emission events were found, I can estimate the lower-limit magnitude (M) that we can detect and use for single-station analysis. This is found using the pretest detonation events. The geophone near Cavern 1 produced signals with about an 8:1 signal-to-noise (SN) level for a 3.5-g source. The other geophone signals had much lower SN levels because of spherical spreading and increased system noise. If I assume that a 3:1 SN level is desirable, using cube-root scaling results in a 0.18-g detectable event. To convert this to magnitude, there are many yield-magnitude curves in the literature. Murphy' relates yield and magnitude for various media in the form

$$M = a + b \log y ,$$

where y is the yield in kilotons and a and b are constants determined from regression analysis. For each medium, a varies; however, b is somewhat constant at (b -0.8). Using Evernden's magnitude estimates[5] results in a value, a -3.46. This translates into a lower-limit magnitude of ~ — 2. This is on the order of the local magnitudes determined by Albright and Pearson from the seismic moment.'

Conclusions

A monitoring system consisting of three triaxial geophone packages surrounding a salt cavern was installed at Bayou Choctaw SPR site. The system also included a computer that detected events and digitized the data for analysis. In general, the uphole monitoring system performed satisfactorily during the experiment. The one exception was wind-induced noise at Well 2, which caused many false alarms in the event detection.

The SPR site has a large amount of cultural and environmental noise. The noise sources caused -800 alarms, from which no seismic emission events were detected. If an on-line seismic monitoring system were attempted, it would require a large amount of time by an analyst to scan for and eliminate false alarms.

System performance would be enhanced by better design of the downhole package. The single-arm-clamp configuration used in the experiment induced different frequency responses in each geophone component, thus distorting the signal and precluding any comparisons between components. Thus, the magnitude and location of events could not have been determined if any were detected.

APPENDIX A

Location of Caprock-Salt Interface

To explain the different average velocities listed in Table 3, it must be realized that two media are present. Caprock-salt interface locations at the various holes are listed in Table Al as given by a geological log.

Table Al. Salt-Caprock Interface Depths

Hole	Depth
Borehole 2	646 ft
Well 1	653 ft
Well 2	639 ft
Well 3	660 ft

The caprock velocity is calculated from the time between the detonation shot at 600 ft deep and its detection at the Well 4 geophone: The salt velocity is calculated from the time between the detonation shot at 700 ft and its detection at the Well 1 geophone. Any ray path that interacts with the salt-caprock interface will result in an average velocity between the caprock velocity and the salt velocity.

Figure Al shows the ray path for two homogeneous half spaces in which the source (s) is in the lower medium and a receiver (r) is in the upper medium. This path can be described by a set of equations,

$$t = H_1/v_1 \cos_1 + H_2/v_2 \cos \theta_2 ,$$

$$x = H_1 \tan \theta_1 + H_2 \tan \theta_2 ,$$

$$\frac{\sin \theta_1}{v_1} = \frac{\sin \theta_2}{v_2} ,$$

$$H = H_1 + H_2 ,$$

where t is the time difference of the path, x is the range, v_1 and v_2 are the p-wave velocities in each medium, and H_1 and H_2 are interface distances for the shot and receiver. For our situation, the known quantities are t, x, H, v_1, and v_2. The unknowns are H,, H,, θ_1, and θ_2. This set of equations can be solved by eliminating H_1 and H_2 and using Newton's method to solve for either θ_1 or θ_2. Table A2 shows the arrival times for each path.

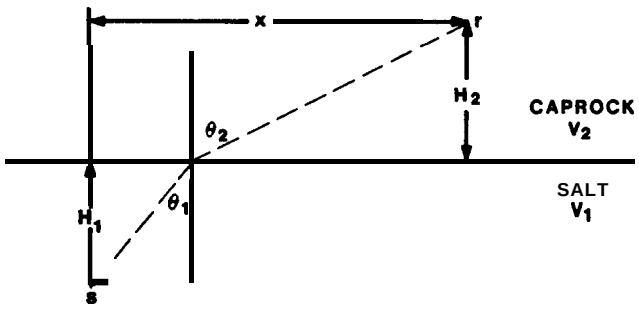

Figure Al. Ray Path of Source (s) to Receiver (r)

The result of the calculation for the 700-ft detonation shows the interface at 636 ft. This seems reasonable; however, the 600-ft detonation calculation shows the interface at 666 ft. To make the results consistent, the 600-ft event would have to be at the 620-ft level. If this were true, the interface would calculate to 637 ft deep. It seems possible that the depth of this event was misplaced by 20 ft.

Table A2. Data Used In the Calculation of Salt-Caprock Interface Depth

	T (Samples)	AT (Samples)	$\bar{V}$ (ft/s)
	Event at 700 ft		
Well 4	7329	185	16 235
Well 1	7285	141	14 485
Borehole 1	7342	248	14 515
Shot Time	7144	0	
	Event at 620 ft		
Well 4	7112	177	16 923
Well 1	7087	150	14 846
Shot Time	6937	0	

Event at 700 ft, H_2 = 635.5 ft

Event at 620 ft, H_2 = 637.1 ft

APPENDIX B

Induced Frequencies Resulting From Mechanical Coupling of the Geophone Package to the Borehole

A possible explanation of the anomalous frequencies shown on the records can be made if we assume that the clamping arm is a vibrating beam and is mechanically inducing certain frequencies into the system. In this section, I calculate normal mode solutions for a beam by using various boundary conditions and attempt to show that the resultant frequencies are approximately the dominant frequencies in the recorded signals.

Let us first review the geometry of the clamping arm and the alignment of the geophones relative to the arm. As noted previously, the clamping arm extends out of the geophone package and pushes against the side of the hole. Both the vertical and the radial components lie in the plane of this extension, and as far as the beam vibrations are concerned, both components should "see" the same frequencies. The tangential component is normal to this extension plane, and because of the different beam dimensions, it should see different, but predictable, frequencies than do the vertical and radial components.

Two different types of boundary conditions are considered. These include the clamped and freely hinged boundary conditions. The freely hinged boundary conditions are probably the most realistic, but since both conditions produce frequencies in the range of interest and the calculations are not unduly complicated, they are both considered.

The clamped boundary conditions specify the vanishing of the displacement and its first derivative at a point; i.e.,

$$u\Big|_{x-x,} = 0 \text{ and } \frac{du}{dx}\Big|_{x=x_o} = 0 \ . \qquad \text{(B1)}$$

This says that the beam is rigidly embedded at point x_o such that there is no displacement and the slope of the beam at that point is always zero.

The freely hinged boundary condition also gives the displacement as zero, but with the second condition of a vanishing second derivative at a point; i.e.,

$$u\Big|_{x=x_o} = 0 \text{ and } \frac{d^2u}{dx^2}\Big|_{x=x_o} = 0 \ . \qquad \text{(B2)}$$

The second derivative (d^2u/dx^2) is proportional to the flexural couple about this point. Thus, although the point is fixed, this couple vanishes.

The standard equation of motion for a vibrating beam is given as[6]

$$\rho \frac{\partial^2 u}{\partial t^2} = -E\ g^2 \frac{\partial^4 u}{\partial s^4} \qquad \text{(B3)}$$

where

ρ = density,
E = Young's modulus,
g = radius of gyration of the cross section of an axis, through its centroid at right angles to the plane of bending,
u = displacement, and
s is defined in Figure B1.

'For the rectangle in Figure B1, the radius of gyration is

$$g^2 = \frac{b^2}{12}, \qquad \text{(B4)}$$

where b is the thickness of the beam. The equation of motion can be written as

$$\frac{\partial^2 u}{\partial t^2} = -a^2 \frac{\partial^4 u}{\partial s^4}, \qquad \text{(B5)}$$

where

$$a^2 = \frac{E}{\rho} \frac{b^2}{12} \ .$$

The harmonic solution to Eq (B5) is:

$$u = A\cosh\sqrt{\frac{w}{a}}s + B\cos\sqrt{\frac{w}{a}}s + c\sinh\sqrt{\frac{w}{a}}s + D\sin\sqrt{\frac{w}{a}}s, \quad \text{(B6)}$$

where w is the circular frequency.

The clamped boundary conditions at s = 0 are:

$$u = \frac{du}{ds} = 0.$$

This implies that

$$A = -B, \qquad C = -D.$$

Thus,

$$u = A\left(\cosh\sqrt{\frac{w}{a}}s - \cos\sqrt{\frac{w}{a}}s\right) + c\left(\sinh\sqrt{\frac{w}{a}}s - \sin\sqrt{\frac{w}{a}}s\right). \quad \text{(B7)}$$

I will now consider three types of motion with reasonable boundary conditions and calculate the corresponding frequency of the highest mode. This includes the clamped-clamped, clamped-hinged, and hinged-hinged conditions.

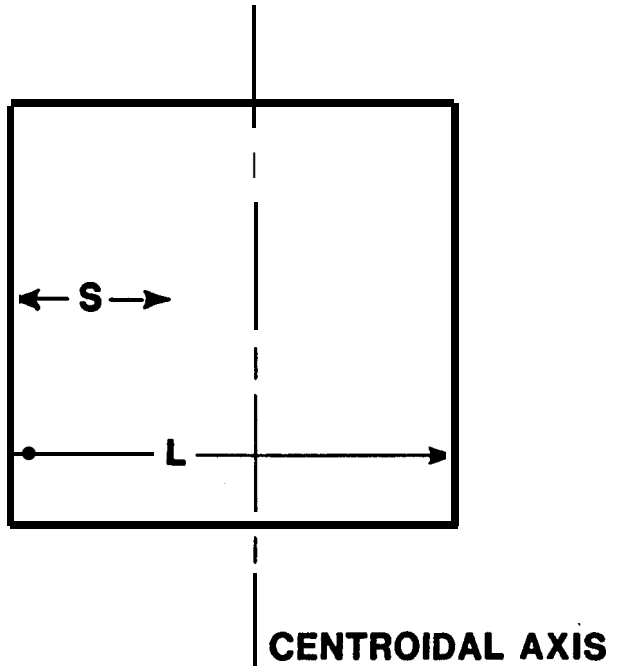

Figure **B1.** Rectangular Model of Clamping Arm

Clamped-Clamped Boundary Conditions

In this case, the clamped boundary condition at the other end of the beam requires

$u = \frac{du}{ds} = 0$ at s = L. L = length of clamping arm. If $\sqrt{\frac{w}{a}}L = z$, and using Eq **(B7),** the resulting characteristic frequency equation is:

$$\cosh z \cos z = 1. \quad \text{(B8)}$$

The approximate lowest mode solution is:

$$z = 4.730.$$

Solving for the angular frequency, w:

$$w = \frac{4.73^2\sqrt{\frac{5}{6}}v_p b}{\sqrt{12}\,L^2}. \quad \text{(B9)}$$

The $\sqrt{\frac{5}{6}}$ is the result of assuming Poisson solid.

In our case for the tangential motion, the approximate values for Eq **(B9)** are:

$$v_p \approx 16\,000 \text{ ft/s}, \quad b \approx 1 \text{ in.}, \quad L \approx 17\text{-}1/4 \text{ in.} \quad \text{(B10)}$$

The frequency f is then

$$f \approx 605 \text{ Hz}.$$

This analysis is also used for the other components since the sole difference between the tangential motion and the radial (or vertical) motion is the result of the different radius of gyration. The width **(b)** of the beam in the radial case is much larger, 3.375 in. This results in a much stiffer beam and a higher frequency; i.e., f = 2000 Hz.

Hinged-Clamped Boundary Conditions

Lower frequencies can be generated by assuming one end is clamped and the other end is hinged. The hinged boundary conditions are:

$$u = \frac{d^2u}{ds^2} = 0 \text{ at } s = L.$$

Again, using Eq (B7) and the above conditions, I obtain a frequency equation of the form

$$\tanh z = \tan z, \qquad \text{(B11)}$$

where we used the same notation as previously designated. The lowest mode solution is:

$$z = 3.93.$$

Again, using the appropriate values results in frequencies of 417 Hz and 1400 Hz for the tangential and radial cases, respectively.

Hinged-Hinged Boundary Conditions

Perhaps a more realistic boundary condition is the beam freely hinged at both ends. This requires using Eq (B2) at both ends of the arm. Under these conditions, the frequency Eq (B6) becomes:

$$\sin \sqrt{\frac{w}{a}} L = 0.$$

This expression leads to frequencies of 267 Hz and 900 Hz for the tangential and radial cases. These frequencies are quite close to the dominant frequencies in Figures 20 and 21, i.e., 200 Hz and 850 Hz, respectively. Thus, it seems conceivable that the clamping-arm frequency response is inducing its frequencies into the signal. Table B1 gives all of the results calculated thus far.

Table B1. Frequencies in Three Boundary Conditions

	Radial and Vertical	Tangential
Clamped-Clamped	2000 Hz	605 Hz
Clamped-Hinged	1400 Hz	417 Hz
Hinged-Hinged	900 Hz	267 Hz

As a final result, I can make a calculation of the tangential motion that results in a frequency closer to the 200 Hz value found in Figure 20. The clamping arm is not an idealized rectangular beam, but has a rather complicated geometry. A section is removed from the clamp to allow it to be hinged when the arm is extended (Figure B2). Thus, we are dealing with a compound beam in which the two sections have different radii of gyration. This cutout section has no effect on the radial motion since its vibrations are parallel to the removed section.

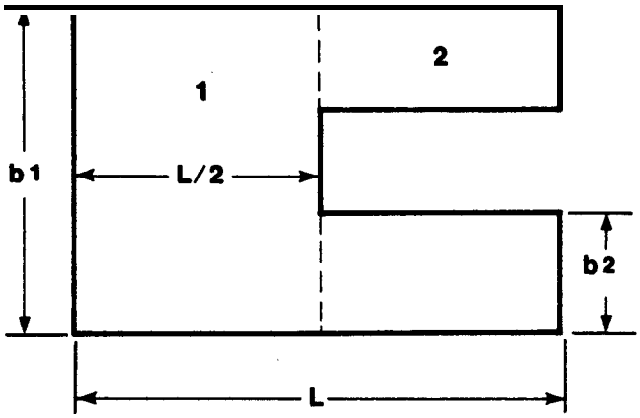

Figure B2. Model of Hinged Clamping Arm

The frequency of the system in Figure B2 can be determined by using the Rayleigh-Ritz method. The section to the left (designated by 1) satisfies the beam Eq (B1):

$$\rho \frac{\partial^2 u}{\partial t^2} = - E g_1^2 \frac{\partial^4 u}{\partial s^4}.$$

On the right, this section satisfies

$$\rho \frac{\partial^2 u}{\partial t^2} = - E g_2^2 \frac{\partial^4 u}{\partial s^4}.$$

Multiplying each of these equations by $\frac{\partial u}{\partial t}$, summing, and integrating over time period and volume, the average kinetic energy is formed:

$$T = \frac{1}{2}\int_0^L dx\,(\rho w^2 u^2)$$

$$= + E g_1^2 \int_0^{\frac{L}{2}} -\frac{1}{2} u \frac{\partial^4 u}{\partial x^4} dx + E g_2^2 \int_0^{\frac{L}{2}} \frac{1}{2} u \frac{\partial^4 u}{\partial x^4} dx.$$

Solving this for the circular frequency gives:

$$w^2 = \frac{a_1^2 \int_0^{\frac{L}{2}} u \frac{d^4 u}{dx^4} dx + a_2^2 \int_0^{\frac{L}{2}} u \frac{d^4 u}{dx^4} dx}{\int_0^L u^2 dx}$$

An appropriate guess for a lowest mode u solution is:

$$u = A L^4 \left\{ \left(\frac{x}{L}\right)^4 - 2\left(\frac{x}{L}\right)^3 + \left(\frac{x}{L}\right) \right\}.$$

It can be shown that this particular expression satisfies the free-hinged boundary conditions. If this expression is put into the above relation for b_1 = 1 in. and b_2 = 1/4 in., the frequency of 195 Hz is found.

References

[1]J. N. Albright and *C.* F. Pearson, ***Microseismic Monitoring at the Bryan Mound Strategic Petroleum Reserve*** (New Orleans, LA: DOE, Office of Strategic Petroleum Reserves, 15 Mar 1979).

[2]P. D. Merillat and A. G. Bauer, ***Strategic Petroleum Reserve Acquisition System,*** SAND80–2143 (Albuquerque, NM: Sandia National Laboratories, Oct 1960).

[3]J. N. Brune, "Tectonic Stress and the Spectra of Seismic Shear Waves from Earthquakes," ***J Geophys Res*** 75:4997-5009 (1970).

[4]J. R. Murphy and R. A. Mueller, "Seismic Characteristics of Underground Nuclear Detonations. Part II, Elastic Energy and Magnitude Determinations," ***Bull Seism Soc Am*** 61:1693-1704 0971).

[5]J. F. Evernden and D. M. Clark, 'Study of Teleseismic P II Amplitude Data," ***Phys Earth Planet Interiors*** 4:24-31 (1970).

[6]A. E. H. ***Love, A Treatise on the Mathematical Theory of Elasticity (New*** York, NY: Dover, 1944), pp 427-43.

DISTRIBUTION:

US Department of Energy SPR PMO (8)
Attn: E. E. Chapple, PMO-581 (6)
TDCS, L. Smith (2)
900 Commerce Road East
New Orleans, LA 70123

US Department of Energy (2)
Strategic Petroleum Reserve
Attn: D. Johnson
D. Smith
1000 Independence Avenue SW
Washington, DC 20585

US Department of Energy
Oak Ridge Operations Office
Attn: P. Brewington, Jr.
PO Box E
Oak Ridge, TN 37631

Aerospace Corporation (2)
Attn: K. Henrie
R. Merkle
800 Commerce Road East, Suite 300
New Orleans, LA 70123

Walk-Haydel & Associates
Attn: R. Haney
600 Carondelet
New Orleans, LA 70112

POSSI (2)
Attn: K. Mills
850 S. Clearview Pkwy
New Orleans, LA 70123

5233	J. P. Holmes
6200	V. L. Dugan
6250	B. W. Marshall
6257	R. R. Beasley
6257	J. K. Linn (10)
6257	C. A. Searls
6257	J. L. Todd
7100	C. D. Broyles
7110	J. D. Plimpton
7111	J. R. Banister
7111	L. J. Barrows
7111	H. D. Garbin (15)
7111	L. J. Vortman
7112	C. R. Mehl
7120	T. L. Pace
7123	G. L. Miller
7137	B. C. Benjamin
7137	R. V. Peet
8024	M. A. Pound
3141	C. M. Ostrander (5)
3151	W. L. Garner (3)
3154-3	C. H. Dalin (25)
	DOE/TIC (Unlimited Release)